Shape from Focus: An Effective Approach for Rough Surfaces

Shree K. Nayar

The Robotics Institute
Dept. of Electrical and Computer Engineering
Carnegie Mellon University
Pittsburgh, Pennsylvania 15213, U.S.A

Yasuo Nakagawa

Production Engineering Research Laboratory
Hitachi Ltd.
292 Yoshida-Machi, Totsuka-Ku
Yokohama 244, Japan

Abstract

Rough surfaces pose a challenging shape extraction problem. Images of rough surfaces are often characterized by high frequency intensity variations, and it is difficult to perceive the shapes of these surfaces from their images. The *shape-from-focus* method described in this paper uses different focus levels to obtain a sequence of object images. The sum-modified-Laplacian (SML) operator is developed to compute local measures of the quality of image focus. The SML operator is applied to the image sequence, and the focus measures obtained at each image point are used to compute local depth estimates. We present two algorithms for depth estimation. The first algorithm simply looks for the focus level that maximizes the focus measure at each image point. The second algorithm uses a Gaussian model to interpolate the focus measures to obtain more accurate depth estimates. The algorithms were implemented and tested on surfaces of different roughness and reflectance properties. The results indicate that the shape-from-focus method may be applied to a variety of industrial vision problems.

1 Introduction

1.1 Motivation

The advancement of three-dimensional machine vision is largely dependent on the development of efficient and reliable shape extraction methods. Shape extraction, in turn, requires a sound understanding of various surface reflection mechanisms and the image formation process. Many extraction methods, for diffuse and specular surfaces, have been developed in the past. However, the extraction problem associated with *rough* surfaces has not received sufficient attention. All surfaces encountered in practice are rough at some level detail. At that level, they exhibit high frequency spatial surface variations that are often random in nature. In many vision applications, the spatial surface variations are comparable in dimensions to the viewing area of individual picture elements of the imaging sensor. Hence, image intensities produced by such surfaces vary in an unpredictable manner from one sensor element to the next, and it is difficult to obtain dense and accurate surface shape information by using existing techniques, such as, structured light, shape-from-shading, stereopsis, etc. Therefore, a practical and reliable solution to this rather difficult extraction problem is desirable.

1.2 Background

We propose to use focus analysis to recover the shapes of surfaces. Previously, focus analysis has been used to automatically focus imaging systems or to obtain *sparse* depth information from the observed scene. Horn [1] proposed focusing imaging systems by using the Fourier transform and analyzing the frequency content in the image. Tenenbaum [2] developed the gradient magnitude maximization method that uses the sharpness of edges to optimize focus quality. Jarvis [3] proposed the sum-modulus-difference that is computed by summing the first intensity differences between neighboring pixels along a scan-line and is used as a measure of focus quality. Schlag et.al. [4] implemented and tested various automatically focusing algorithms.

More recently, Krotkov [5][6] evaluated and compared the performance of different focus criterion functions. Krotkov also proposed a method to estimate the depth of an image area. Pentland [7] suggested estimating the depth of image points by evaluating image blur due to defocusing. Grossmann [8] has proposed estimating depth of edge points by analyzing the blur of edges. Darrell and Wohn [9] have developed a depth from focus method that obtains an image sequence by varying the focus level and uses Laplacian and Gaussian pyramids to calculate depth. Subbarao [10] suggests the change of intrinsic camera parameters to recover the depth map of a scene. Ohta et.al. [11] and Kaneda et.al. [12] have used images corresponding to different focus levels to obtain a single level of high focus quality.

1.3 Proposed Approach

In this paper, we develop a shape-from-focus method. In contrast to previous work in this area, we avoid the following approaches.

- We will not attempt to estimate depth from a pair of images by evaluating local estimates of the blurring function. The accuracy of such a method is greatly dependent on the blurring model used. The models used thus far are only approximations to the actual physical-optics model and therefore do not ensure high quality results.
- We will not apply our method to general scenes. Depth estimation based on focus analysis relies on the presence of some high frequency brightness variation in the scene. General scenes often have areas with little or no brightness variation. For this reason, experiments in the past have only produced sparse depth information.

We restrict ourselves to visibly rough surfaces that produce textured images with high frequency intensity variations. We review the image formation process and show that a defocused imaging system plays the role of a low-pass filter. The shape-from-focus method moves the unknown object with respect to the imaging system and obtains a sequence of images that correspond to different levels of object focus. The sum-modified-Laplacian (SML) focus operator is developed to measure the relative degree of focus between images. The operator is applied to the image sequence to obtain a set of focus measures at each image point. The focus measure values at each point are modeled and interpolated to obtain accurate depth estimates. Experimental results indicate that the method is capable of extracting *dense and accurate* shape information with appreciable invariance to texture strength and type.

2 Visibly Rough Surfaces

In the study of reflection, a rough surface is defined as one whose smallest spatial variations have dimensions that are much larger than the wavelength of the incident electromagnetic wave. This is the concept of optical roughness. In this paper, we introduce the notion of *visible roughness*; a surface is considered to be rough if the dimensions of its spatial variations are comparable to the viewing area of individual elements (e.g. pixels) of the sensor (e.g. camera) used to observe the surface. The surface shown in Fig.1 is composed of a large num-

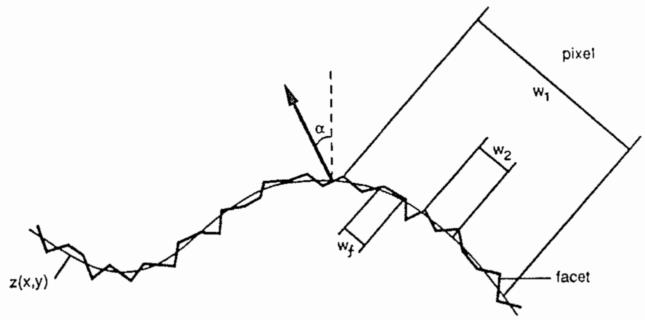

Figure 1: Rough Surface.

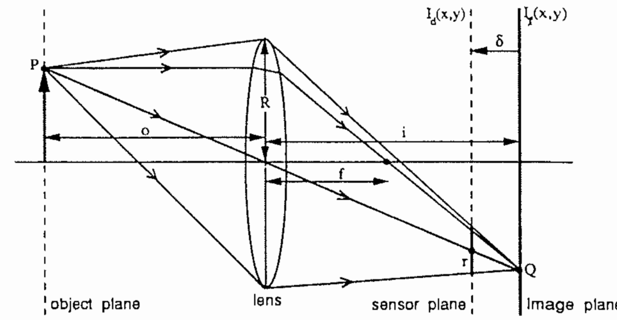

Figure 2: Formation of focused and defocused images.

ber of facets[1]. While the surface appears to have a smoothly varying global shape, $z(x, y)$, the orientation α of individual facets may deviate substantially from the mean surface orientation in the facet vicinity. Although facet orientations are dependent on the global shape of the surface and on the orientations of neighboring facets, they may exhibit some degree of randomness.

Now let us consider the image of a rough surface generated by using a finite resolution sensor. The number of facets that contribute to the image irradiance at a pixel location depends on the magnification of the optics used to project the surface onto the image plane of the sensor. We define two levels of magnification; *multi-facet level* and *facet level*. At the multi-facet level, the pixel width w is very large compared to the facet size w_f (e.g. $w = w_1$). In this case, the surface patch projected on a pixel may be modeled by assigning it a mean orientation value and a roughness which is determined by the probability function of its facet orientations [13] [14]. The pixel intensities are continuous functions of the angle of incident light and can be expressed as a linear combination of the diffuse lobe and specular lobe components [14], the relative strengths of the two components depending on the reflectance properties of the facets.

At facet level magnification, on the other hand, the pixel width w is comparable to the facet width w_f (e.g. $w = w_2$), and only one or few facets are viewed by each pixel. As a result of the random nature of facet orientations, image intensity values are expected to vary drastically and unpredictably from one pixel to the next. This is true for both specular as well as diffuse facets as the radiance of both are dependent on the angle of incident light. Therefore, at the facet level, the surface produces images that are rich in *texture*[2] and we say that the surface is *visibly rough*. But, why do we use facet level measurements when multi-facet level measurements will provide us with image intensities that can perhaps be used to extract shape information? In many practical instances, the desirable resolution of shape information is unobtainable at the multi-facet level.

3 Focused and Defocused Images

In this section, we briefly review the image formation process and describe defocused images as processed versions of focused images. Fig.2 shows the basic image formation geometry. All light rays that are radiated by the object P and intercepted by the lens are refracted by the lens to converge at the point Q on the image plane. The relationship between the object distance o, focal distance of the lens f, and the image distance i, is given by the Gaussian lens law:

$$\frac{1}{o} + \frac{1}{i} = \frac{1}{f}. \tag{1}$$

Each point on the object plane is projected onto a single point on the image plane, thus causing a clear or *focused* image $I_f(x,y)$ to be formed on the image plane. If, however, the sensor plane does not coincide with the image plane and is displaced from the image plane by a distance δ, the energy received from the object by the lens is distributed over a circular[3] patch on the sensor plane. Fig.2 may be used to establish the relationship between the radius r of the circular patch and the sensor displacement δ. By using similar triangles, we find that:

$$r = \frac{\delta R}{i} \tag{2}$$

where R is the radius of the lens. It is also possible to convince oneself that the radius r of the circular patch is independent of P's location on the object plane. The distribution of light energy over the circular patch, or the *blurring function*, can be modeled using physical optics [17]. Very often, a two-dimensional Gaussian function is used to approximate the physical model [7]. Then, the blurred or *defocused* image $I_d(x, y)$ formed on the sensor plane can also be determined by convolving the focused image $I_f(x, y)$ with the blurring function $h(x, y)$:

$$I_d(x, y) = h(x, y) * I_f(x, y) \tag{3}$$

where:

$$h(x, y) = \frac{1}{2\pi\sigma_h^2} e^{-\frac{x^2+y^2}{2\sigma_h^2}} \tag{4}$$

where σ_h, the *spread parameter*, is assumed to be proportional to the radius r [7]. The constant of proportionality is dependent on the optics, sampling, etc. We will see shortly that the value of this constant is not important in our approach. Note that defocusing is observed for both positive and negative sensor displacements.

Now let us analyze the defocusing process in the frequency domain (u, v). If $I_F(u, v)$, $H(u, v)$, and $I_D(u, v)$ are the Fourier transforms of $I_f(x, y)$, $h(x, y)$, and $I_d(x, y)$, respectively, we can express eq.3 as:

$$I_D(u, v) = H(u, v) \,.\, I_F(u, v) \tag{5}$$

where:

$$H(u, v) = e^{-\frac{u^2+v^2}{2}\sigma_h^2} \tag{6}$$

We see that $H(u, v)$ allows low frequencies to pass while it attenuates the high frequencies in the focused image. Furthermore, as the sensor displacement δ increases, the defocusing radius r increases, and the spread parameter σ_h increases. Hence defocusing is a *low-pass* filtering process where the bandwidth decreases with increase in defocusing.

From Fig.2, it is seen that a defocused image of the object can be obtained in three ways: by displacing the sensor with respect to the image plane, by moving the lens, or by moving the object with respect to the object plane. Moving the lens or sensor plane with respect to one another causes the following problems:

- The magnification of the system varies, thereby causing the image coordinates of the object points to change.
- The area on the sensor plane over which light energy is distributed varies, thereby causing a variation in image brightness.

[1]No assumptions are made regarding the size of the facets. Hence, these facets may or may not represent the *micro-facets* defined in [13], [14].

[2]There are many notions of what is meant by the term texture. Here, we define texture as a noticeable fluctuation in the intensities of neighboring image pixels [18]. The textures produced by rough surfaces may be periodic, nearly periodic, or random. No assumptions are made regarding the type of texture.

[3]The shape of the patch also depends on the shape of the aperture of the imaging system. We are assuming the aperture to be circular.

In order to overcome these problems, we propose to vary the degree of focus by moving the object[4] with respect to a fixed configuration of the optical system and sensor. This approach ensures that the focused areas of the image are always subjected to the same magnification.

4 Shape from Focus: An Overview

The shape-from-focus method is based on the observations made in the previous sections.

- At facet level magnification, rough surfaces produce images that are rich in texture.
- A defocused optical system plays the role of a low-pass filter.

Fig.3 shows a rough surface of unknown shape placed on a translational stage. The reference plane shown corresponds to the initial position of the stage. The configuration of the optics and sensor defines a single plane, the "focused[5] plane," that is perfectly focused onto the sensor plane. The distance d_f between the focused and reference planes, and the displacement d of the stage with respect to the reference plane, are always known by measurement. Consider the surface element, s, that lies on the unknown surface, S. If the stage is moved towards the focused plane, the image will gradually increase in its degree of focus (high frequency content) and will be perfectly focused when s lies on the focused plane. Further movement of the element s will again increase the defocusing of its image. If we observe the image area corresponding to s and record the stage displacement $d = \bar{d}$ at the instant of maximum focus, we can compute the height d_s of s with respect to the stage as $d_s = d_f - \bar{d}$. In fact, we can use $\bar{d}$ to determine the distance of s with respect to the focused plane, sensor plane, or any other coordinate system defined with respect to the imaging system. This approach may be applied independently to all surface elements to obtain the shape of the entire surface S.

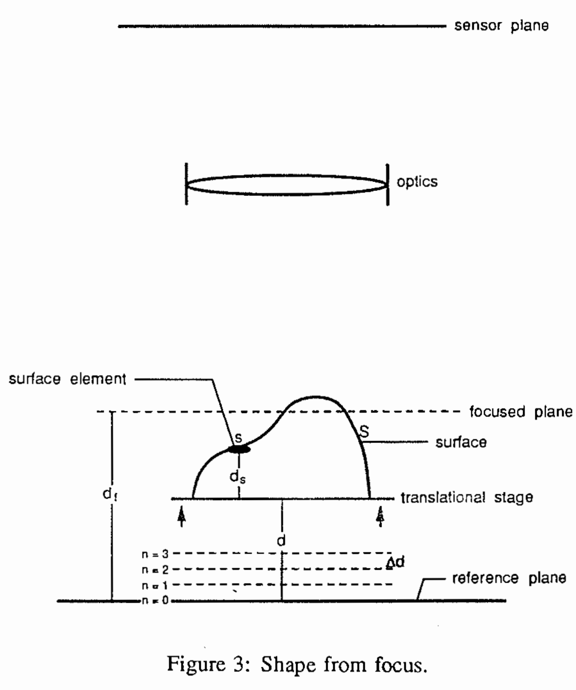

Figure 3: Shape from focus.

[4]Object movement is easily realized in industrial inspection applications.

[5]The focused plane is the same as the object plane defined in the previous section. A different name is used here as the object does not necessarily lie on the focused plane.

5 A Focus Measure Operator

To automatically detect the instant of "best" focus, we will develop a focus measure operator. The operator must respond to high frequency variations in image intensity, and ideally, must produce maximum response when the image area is perfectly focused. The high frequency content of an image area can be determined by using the Fourier transform and analyzing the frequency distribution. However, since Fourier transforms are expensive to compute without special purpose hardware, we seek an alternative method.

A few focus measure operators have been proposed and used in the past [5]. Generally, the objective has been to find an operator that behaves in a stable and robust manner over a variety of images such as images of outdoor scenes, text, etc. Such an approach is essential while developing automatically focusing imaging systems that have to deal with "general" scenes. Bearing in mind that we are dealing with textured images, we develop an operator that is particularly well-suited to such images. In the next section we will evaluate the performance of our operator.

One way to high-pass filter an image is to determine its second derivative. For two-dimensional images, the *Laplacian* is very often used:

$$\Delta^2 I = \frac{\partial^2 I}{\partial x^2} + \frac{\partial^2 I}{\partial y^2} \tag{7}$$

where $I(x,y)$ is the image intensity at the point (x,y). In frequency domain, applying the Laplacian $L(u,v)$ to the defocused image $I_D(u,v)$ (equation 5) gives:

$$L(u,v) \,.\, H(u,v) \,.\, I_F(u,v) \tag{8}$$

where:

$$L(u,v) \,.\, H(u,v) = -(u^2+v^2) \,.\, e^{-\frac{u^2+v^2}{2}\sigma_h^2} \tag{9}$$

Fig.4 shows the frequency distribution of $| L.H |$ as a function of the defocusing parameter σ_h. The Laplacian acts as a high-pass filter and makes the effect of defocusing on the high frequencies prominent. Interestingly, for any given frequency (u,v), $| L.H |$ varies as a Gaussian function of the defocusing parameter σ_h. In general, however, the result would depend on the frequency distribution of the imaged scene. Though our texture is random, it may be assumed to have a set of dominant frequencies. Then, loosely speaking, each frequency is attenuated by a Gaussian function in σ_h with a variance that is determined by the frequency. Therefore, the result of applying the Laplacian operator may be expressed as a sum of Gaussian functions in σ_h. The result is expected to be maximum when $\sigma_h = 0$, i.e. when the image is perfectly focused and attenuation for all frequencies is minimum. Since the frequency distribution of the texture is random, the variances of the Gaussian functions are also random. Using cen-

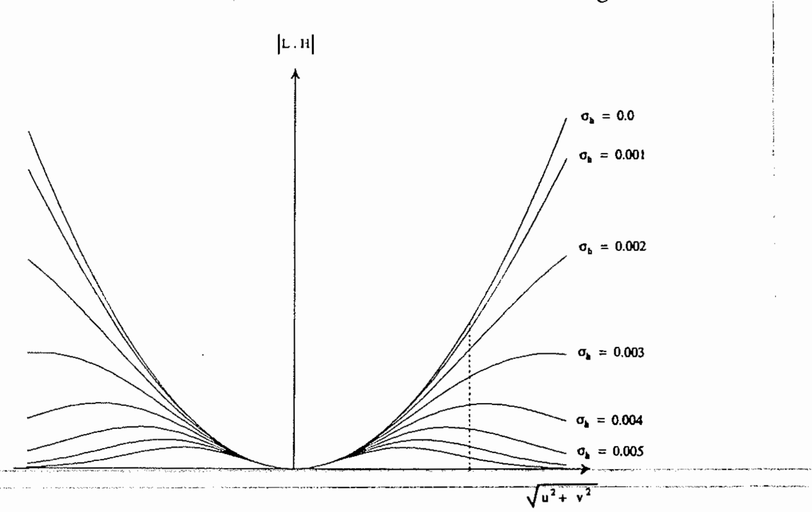

Figure 4: The effect of defocusing and second-order differentiation in frequency domain.

tral limit theorem, the net result may be assumed to be a Gaussian function of the defocusing parameter σ_h. *This general behavior is expected irrespective of the focus measure operator used.* The focus measure operator basically selects the frequencies that will play a dominant role in this process. Both, our own experiments (section 5) and Krotkov's empirical evaluation of various focus measure operators [5] support the above argument. As seen in [5], image noise that is time-varying will of course degrade the performance any focus measure operator.

We note that in the case of the Laplacian the second derivatives in the x and y directions can have opposite signs and tend to cancel each other. An example of such an instance is illustrated in Fig.5; the

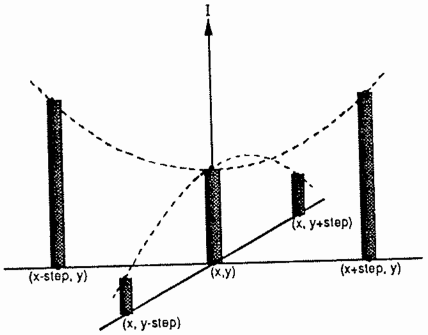

Figure 5: A texture instance with zero Laplacian value.

partial derivatives are equal in magnitude but opposing in sign, i.e. $\Delta^2 I = 0$. In the case of textured images, this and similar instances may occur frequently and the Laplacian is prone to behave in an unstable manner. We overcome this problem by defining the *modified Laplacian* as:

$$\Delta^2{}_M I = \left|\frac{\partial^2 I}{\partial x^2}\right| + \left|\frac{\partial^2 I}{\partial y^2}\right| \qquad (10)$$

Note that the modified Laplacian is always greater or equal in magnitude to the Laplacian. In [15], we have empirically demonstrated the benefits of the above modification. However, the experiments described in [15] also indicate that the response of the modified Laplacian is slightly more stable but not very different from that of the Laplacian.

The discrete approximation to the Laplacian is usually a 3×3 operator. In order to accommodate for possible variations in the size of texture elements, we compute the partial derivatives by using a variable spacing (*step*) between the pixels used to compute the derivatives. Hence, the discrete approximation to the modified Laplacian is computed as:

$$\begin{aligned} ML(x,y) &= \mid 2I(x,y) - I(x-step,y) - I(x+step,y) \mid \\ &+ \mid 2I(x,y) - I(x,y-step) - I(x,y+step) \mid \end{aligned} \qquad (11)$$

Finally, the focus measure at a point (i,j) is computed as the sum of modified Laplacian values, in a "small" window around (i,j), that are greater than a threshold value:

$$F(i,j) = \sum_{x=i-N}^{i+N} \sum_{y=j-N}^{j+N} ML(x,y) \quad for\ ML(x,y) \geq T_1 \qquad (12)$$

where the parameter N determines the window size used to compute the focus measure. In contrast to auto-focusing methods, we typically use a small window of size 3×3 or 5×5, i.e. $N = 1$ or $N = 2$. We shall refer to the above focus measure as the *sum-modified-Laplacian* (SML).

6 Evaluating the Focus Measure

We evaluate the SML focus measure by analyzing its behavior as a function of the distance between the observed surface and the focused plane. A detailed description of the experimental set-up is given in a later section. In the following experiments, texture samples are attached to a translational stage (Fig.3) and the distance, d_s, from each sample to the stage is known by measurement. Images of the samples are obtained using a microscope and a 256×256 pixel CCD camera. The complete imaging system has a physical resolution of approximately $1\mu m$ per pixel width.

In Fig.6, the focus measure functions of two samples are shown. Sample X has high texture content while sample Y has relatively weaker texture. Both samples are made of a paste containing resin and tungsten particles. The variable size of the tungsten particles gives the surfaces a randomly textured appearance. For each sample, the stage is moved in increments (Δd) of $1\mu m$, an image of the sample is obtained, and the focus measure is computed using an evaluation window size of 10×10 pixels. The vertical lines in Fig.6 indicate the known initial distances (d_f - d_s) of the samples from the focused plane. The focus measures were computed using parameter values of $step = 1$ and $T_1 = 7$ [15]. No form of temporal filtering was used to reduce the effects of image noise, as we intend to use unfiltered focus measures to estimate the depth of surface points. Though the measure values are slightly noisy, they peak very close to the expected peak positions (vertical lines in Fig.6). We see that the focus measure function peaks sharply for the stronger texture and it peaks relatively slowly and with a lower peak value for the weaker texture. However, the sharpness of the focus measure function depends not only on the texture strength but also the "depth of field" of the imaging system. The depth of field, in turn, depends on the magnification and aperture size of the imaging system. We will assume that the depth of field is constant for all our experiments.

In [15], we have shown how the SML measure is affected by the selection if its parameters *step* and T_1. In [15], we have also empirically compared the SML focus measure with three other measures that have been previously used for auto-focusing: *Tenengrad*, *variance*, and *sum-Laplacian* (SL). These experiments indicate that, among these operators, the SML operator is best suited for measuring the focus quality of textured images.

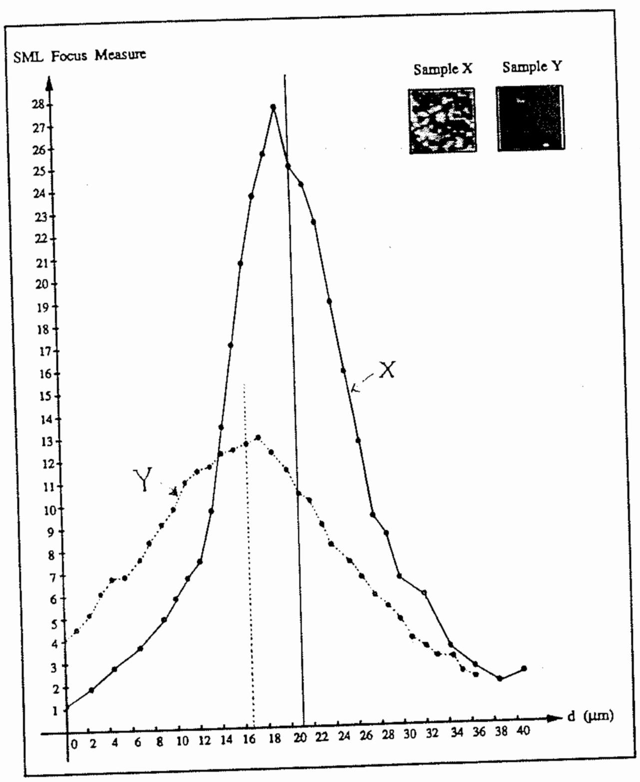

Figure 6: SML focus measure function computed for two texture samples.

7 Sampling the Focus Measure Function

We can represent the focus measure function of an image point (x, y) as $F(x,y,d)$. Since depth estimation is a local operation, we will focus our attention on a single image point, bearing in mind that the same estimation method can be applied to all other image points. Therefore, we will denote the focus measure function as simply $F(d)$. By using the argument presented in section 5 and by studying the experimental result shown in Fig.6, we assume that $F(d)$ has a Gaussian distribution with mean value $\bar{d}$ and standard deviation σ_F (Fig.7). The mean $\bar{d}$ corresponds to the stage displacement at which $F(d)$ is maximum, i.e. $F(\bar{d}) = F_{peak}$. As the texture content of the surface element increases, F_{peak} increases and σ_F decreases. Each surface element, therefore, is expected to have its own F_{peak} and σ_F values.

If we use very small stage displacements ($\Delta d \approx 0$), the number of images to be obtained and processed is too large from the perspective of practical implementation. Hence, we use large displacements to obtain a few images of different focus levels and use the Gaussian model to interpolate the small number of focus measures to obtain depth estimates. Computing focus measures at a finite number of displacements is equivalent to *sampling* the function $F(d)$; at each displacement d_i we compute the focus measure $F(d_i)$ to obtain the set $\{F(d_i) \mid i = 1, 2, \ldots M\}$. We show in the following section that a minimum of *three* focus measures are needed perform the Gaussian interpolation. *In theory, therefore, depth estimates may be obtained from only three images of the surface.* However, since the Gaussian model only approximates the focus measure function, we use the condition $\sigma_F \leq \Delta d \leq 2\sigma_F$ to ensure that evaluation of at least one focus measure in the $\pm\ \sigma_F$ range of $F(d)$. Note that displacements are applied to all object points. Therefore, by applying the above condition to the image area that has maximum texture content, we can ensure that a few or many focus measures will be computed in the $\pm\ \sigma_F$ range at all image points.

We note that the value of σ_F also increases with the depth of field of the imaging system. Therefore, for objects of larger dimensions also, only a small number of images may used by increasing the depth of field.

8 Depth Estimates from Focus Measures

In this section, we describe the estimation of depth of a surface point (x, y) from the focus measure set $\{F(d_i) \mid i = 1, 2, \ldots M\}$. We use the parameter $\bar{d}$ to represent the depth of the surface point. For convenience the notation F_i is used to represent the focus measure value $F(d_i)$. We present algorithms for two different depth estimation methods. Each algorithm may be applied to all points in the image to obtain depth maps.

8.1 Coarse Resolution Depth Estimation

The first algorithm simply looks for the displacement value d_i that maximizes the focus measure and assigns that value to $\bar{d}$.

Algorithm 1

Step 1: Let $k = 1$, $F_{max} = 0$.

Step 2: If $F_k > F_{max}$, $F_{max} = F_k$ and $\bar{d} = d_k$.

Step 3: If $k < M$, $k = k + 1$, go to step 2.

Step 4: If $F_{max} < T_2$, the point (x, y) belongs to *background*. Stop.

This simple algorithm may be used to compute rough depth estimates. The performance of the algorithm is directly dependent on the selection of Δd.

8.2 Depth Estimation by Gaussian Interpolation

The second algorithm uses the Gaussian distribution to model the focus measure function $F(d)$ and interpolates the computed measure values to obtain more accurate depth estimates. One approach is to fit all computed F_i values to the Gaussian model. However, we feel that more accurate depth estimates can be obtained, while saving computations, by using the Gaussian distribution to model only the peak of $F(d)$. The following algorithm uses only three focus measures, namely, F_{m-1}, F_m, and F_{m+1}, that lie on the largest mode of $F(d)$, such that, $F_m > F_{m-1}$ and $F_m > F_{m+1}$ (Fig.7).

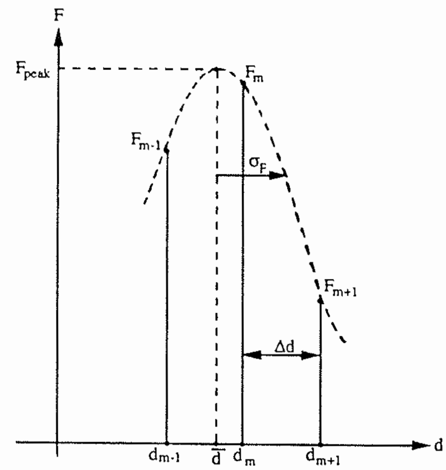

Figure 7: Gaussian interpolation of focus measures.

Using the Gaussian model, the focus measure function may be expressed as:

$$F = F_{peak}\, exp \left\{ -\frac{1}{2}\left(\frac{d - \bar{d}}{\sigma_F}\right)^2 \right\} \tag{13}$$

where $\bar{d}$ and σ_F are the mean and standard deviation of the Gaussian distribution (Fig.7). Using natural logarithm, we can rewrite Eq. 13 as:

$$ln\, F = ln\, F_{peak} - \frac{1}{2}\left(\frac{d - \bar{d}}{\sigma_F}\right)^2 \tag{14}$$

By substituting each of the three measures F_{m-1}, F_m, and F_{m+1}, and its corresponding displacement value in Eq. 14, we obtain three equations that can be solved for $\bar{d}$ and σ_F:

$$\bar{d} = \frac{(ln\,F_m - ln\,F_{m+1})(d_m^2 - d_{m-1}^2) - (ln\,F_m - ln\,F_{m-1})(d_m^2 - d_{m+1}^2)}{2\,\Delta d\{(ln\,F_m - ln\,F_{m-1}) + (ln\,F_m - ln\,F_{m+1})\}} \tag{15}$$

$$\sigma_F^2 = -\frac{(d_m^2 - d_{m-1}^2) + (d_m^2 - d_{m+1}^2)}{2\{(ln\,F_m - ln\,F_{m-1}) + (ln\,F_m - ln\,F_{m+1})\}} \tag{16}$$

Using Eq. 13, we can find F_{peak} from σ_F and $\bar{d}$ as:

$$F_{peak} = F_m \,/\, exp \left\{ -\frac{1}{2}\left(\frac{d_m - \bar{d}}{\sigma_F}\right)^2 \right\} \tag{17}$$

If F_{peak} is large and σ_F is small, the focus measure function has a "strong" peak, indicating high surface texture content in the vicinity of the image point (x, y). Thus, the values of F_{peak} and σ_F can be used to segment the observed scene into regions of different texture content.

The following algorithm first finds the measures F_{m-1}, F_m, and F_{m+1} that correspond to the strongest[6] peak of $F(d)$, and then uses these measures to estimate the depth $\bar{d}$ by Gaussian interpolation.

Algorithm 2

Step 1: Let $k = 3$, $F_{m-1} = 0$, $F_m = 0$, $F_{m+1} = 0$, $d_m = 0$.

[6]Due to image noise and variations in magnification, the focus measure function may be multi-modal with one strong peak and one or more weak ones.

Step 2: If $F_{k-1} > F_m$, $F_{k-1} > F_k$, and $F_{k-1} > F_{k-2}$, then:

$F_m = F_{k-1}$
$F_{m-1} = F_{k-2}$
$F_{m+1} = F_k$
$d_m = d_{k-1}$

Step 3: If $k < M$, $k = k + 1$, go to step 2.

Step 4: $d_{m-1} = d_m - \Delta d$ and $d_{m+1} = d_m + \Delta d$. Determine $\bar{d}$, σ_F, and F_{peak} using Eqs. 15, 16, and 17.

Step 5: If $F_{peak} < T_3$ or $\sigma_F > T_4$, the image point (x, y) belongs to *background*. Stop.

Since the values of F_{peak} and σ_F are only useful for texture classification, their evaluation may be avoided to save computations.

9 Experiments

9.1 Experimental Set-up

Fig.8 shows a photograph of the experimental set-up used to demonstrate the shape-from-focus method. A microscope is used to magnify the object surface and images are obtained using a CCD camera with 256×256 pixels. Camera images are digitized and processes using a computer. The magnification of the imaging system can be varied from ×5 to ×160. The object is placed on a translational stage that is used to move the object through the focused plane of the imaging system. Stage displacements are monitored using an electronic displacement sensor that has an accuracy of within 0.1 μm. In all our experiments, the bright field illumination [15] of the microscope was used to illuminate the object surface.

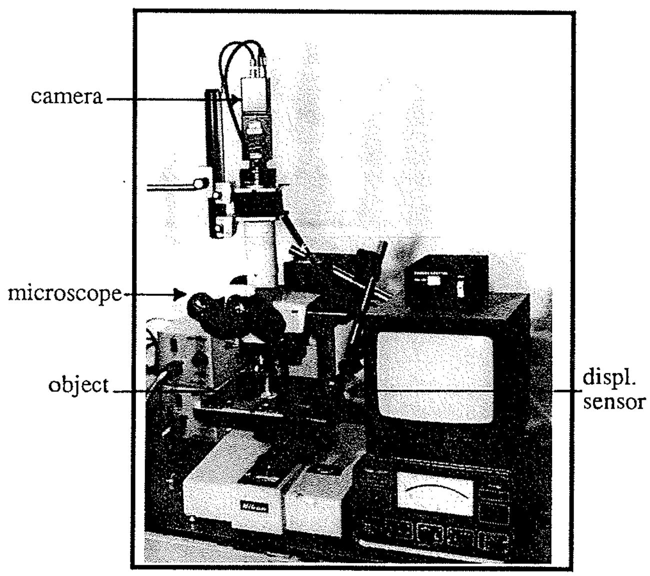

Figure 8: Photograph of the experimental set-up.

9.2 Results

The accuracy of the shape-from-focus algorithms was analyzed using a steel ball sample that was 1590μm in diameter. The ball was sand-papered to give it a rough surface. A camera image of the ball under bright field illumination is shown in Fig.9a. Incremental displacement of Δd = 100 μm were used to obtain 13 images of the ball, and a 5×5 SML operator was applied to the image sequence to obtain focus measures. Depth maps of the ball, generated by the coarse resolution and Gaussian interpolation algorithms, are shown in Fig.9b and 9c, respectively. The known size and location of the ball were used to obtain error maps by subtracting a smooth ball from the two depth maps. It is difficult to define the accuracy of the method as it depends on many factors: the surface texture, depth of field of the imaging system, and the incremental displacement Δd. The table shown in Fig.9d shows the error statistics computed from the error maps corresponding to the two algorithms. A total of 23235 image pixels lie within the boundary of the ball. The number of depth values computes by each algorithm depends on the values selected for the thresholds T_2, T_3, and T_4.

Fig.10 and 11 show samples with different surface reflectance and roughness properties. As it is difficult to perceive the shapes of these samples from their camera images, we have also included scanning electron microscope (SEM) images of the samples. We hope that these images will provide sufficient shape cues to the reader. Both samples are approximately 100 μm in width and an incremental displacement of Δd = 10 μm was used in both cases to obtain sequences of about 10 images each. Depth maps of the samples were obtained using the Gaussian interpolation algorithm. A 5 × 5 median filter was used to get rid of a few erroneous depth estimates that result from the lack of texture in some image areas.

Fig.10a and 10b show the camera and SEM images of a tungsten paste filling in a via-hole on a ceramic substrate [16] that is used to establish electrical connections between different components. Conditions such as excess filling and lack of filling cause electrical defects such as short and open circuits. The sample shown in Fig.10 has a bump on its surface, indicating excess filling. The specular reflectance and variable size of the tungsten particles gives the surface a random texture. The white background (Fig.10a) is the substrate area that has very weak texture. For this sample, we selected the threshold values to classify the substrate area as *background*. An arbitrary depth value is assigned to the background region.

Fig.11 shows another via-hole sample. In this case, the substrate and filling are hardened by baking. The baking process changes the reflectance and texture of the filling and also increases the texture content of the substrate. From the SEM image we see that the via-hole is not sufficiently filled with tungsten paste. For this sample, the algorithm threshold values were selected to obtain the depth of the substrate area too. To accommodate for the large size of substrate texture elements, a *step* size of 2 was used. Two different views of the sample's depth map are shown in Fig.11c.

The above experiments indicate that the Gaussian interpolation algorithm performs stably over a wide range of textures. Errors in computed depth estimates result from factors such as image noise, Gaussian approximation of the SML focus measure function, and weak textures in some image areas. In the current implementation, object displacement and image acquisition are manually initiated. In a high-speed implementation, the object can be moved continuously while images are obtained at fixed intervals of time. By using customized hardware, the SML focus operator can be applied to each image in frame-time and the Gaussian interpolation can be implemented by using look-up tables. We estimate that a high-speed implementation of the method can generate surface depth maps in less than 1 second.

10 Conclusion

In this paper, we have presented shape-from-focus as a new method of extracting the shapes of rough surfaces.

- To measure the quality of image focus we developed the SML operator. By evaluating the SML operator, we found that it is particularly suited for textured images.
- We developed and tested two depth estimation algorithms and found, through numerous experiments, that the Gaussian interpolation algorithm produces accurate results for a variety of textures.
- The local nature of the depth estimation technique enables it to adapt to substantial variations in image texture.
- Though we have concentrated on rough surfaces in this paper, the shape-from-focus method can be directly applied to smooth textured surfaces. Smooth non-textured surfaces can also be handled by using special illumination techniques [15].
- This method may be directly applied to a number of industrial machine vision problems. Our experiments demonstrate one such application, namely, the inspection of via-hole fillings on ceramic substrates.

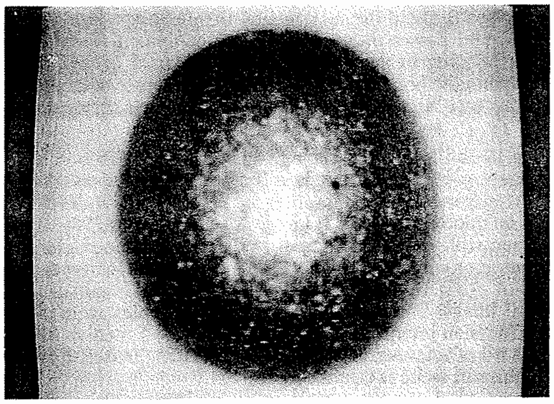

(a) Camera image.

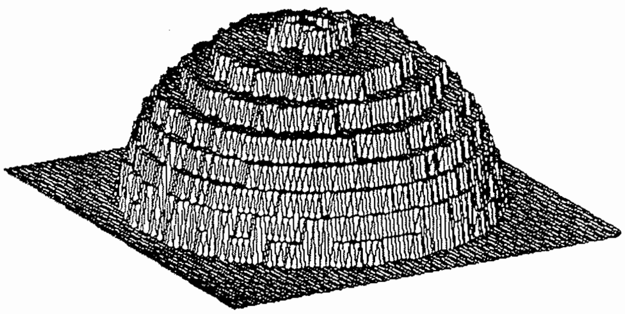

(b) Depth map: coarse resolution.

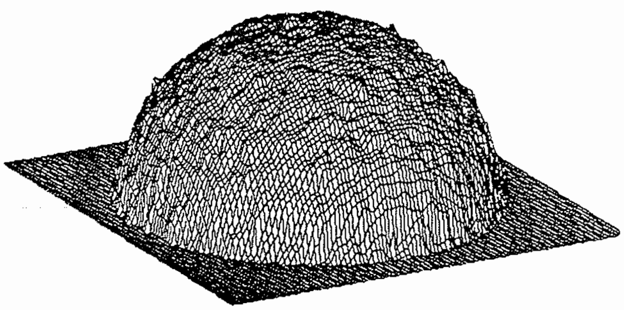

(c) Depth map: Gaussian interpolation.

Diameter of Test Sphere : 1590 μm		
	Coarse	Gaussian Interpolation
Number of Points	22682	23257
Mean Error (μm)	7.861	3.857
Mean Absolute Error (μm)	30.32	13.815
Maximum Absolute Error (μm)	187.80	175.82

(d) Error statistics.

Figure 9: Steel ball.

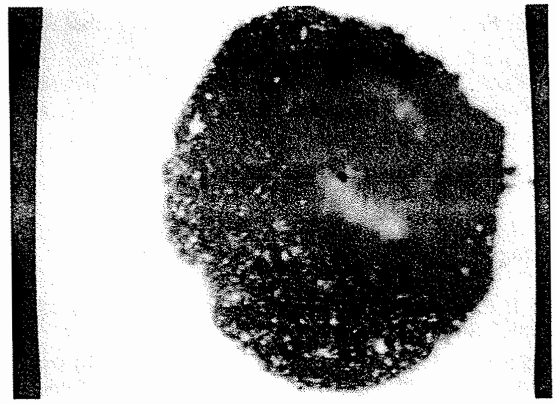

(a) Camera image.

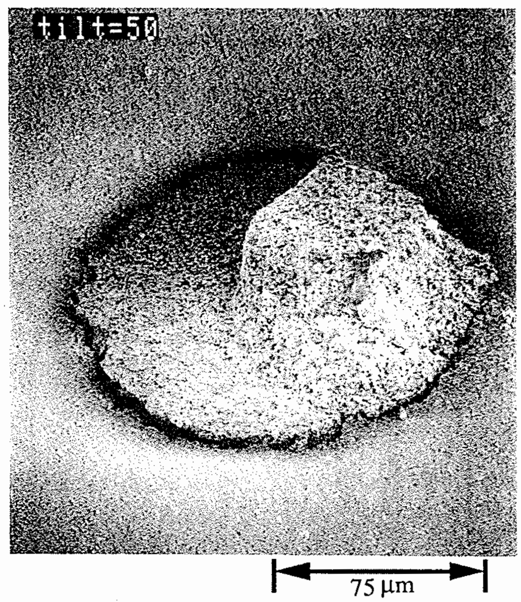

(b) SEM image.

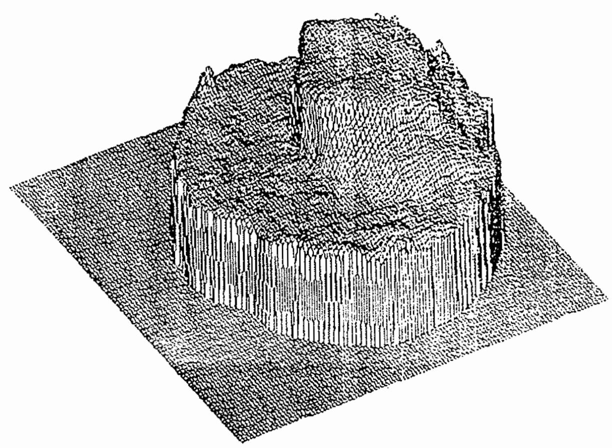

(c) Depth map

Figure 10: Via-hole filling.

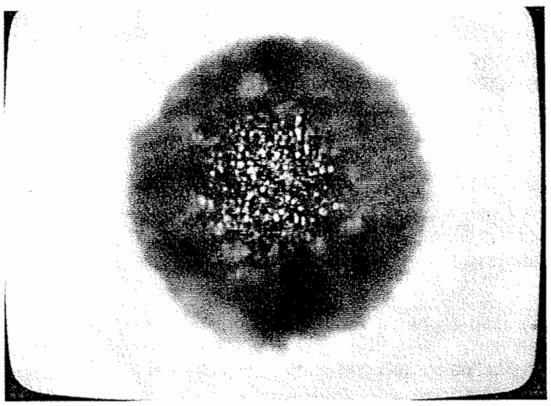

(a) Camera image.

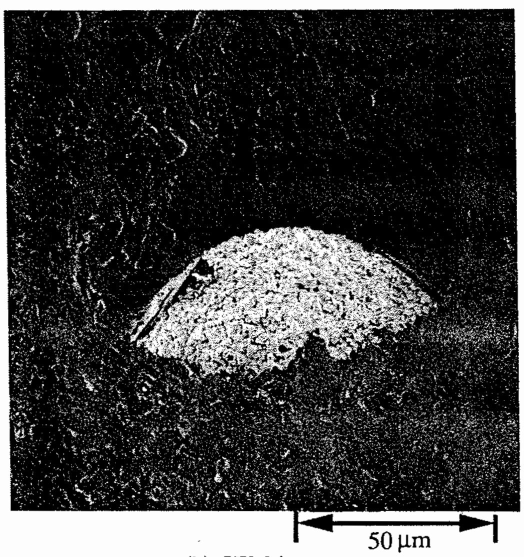

(b) SEM image.

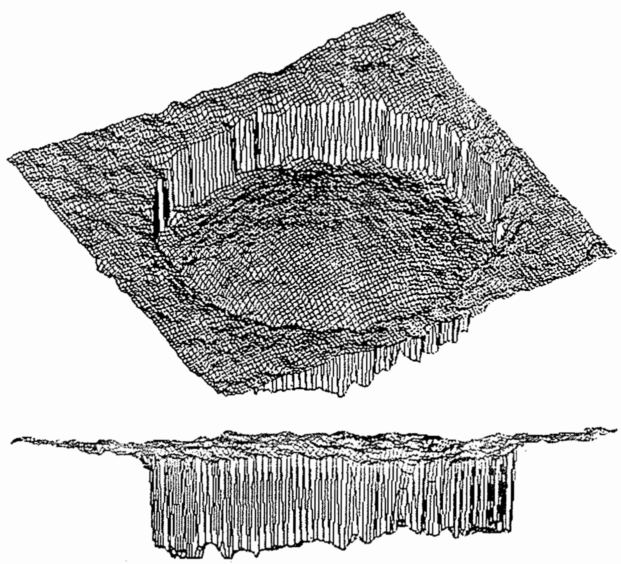

(c) Depth maps.

Figure 11: Baked via-hole filling.

Acknowledgements

This research was supported by and conducted at the Production Engineering Research Lab. (PERL), Hitachi Ltd., Yokohama, Japan, during the first author's visit in the summer of 1989. The authors are grateful to Eric Krotkov for all the valuable information he provided during the initial stages of this effort. Members of the 3.4 Group at PERL, members of the VASC group at CMU, Eric Krotkov, Katsushi Ikeuchi, and Takeo Kanade provided many useful comments. Kathy Porshe read earlier versions of this paper.

References

[1] B.K.P. Horn, *Focusing,* MIT Artificial Intelligence Laboratory, Memo No. 160, May, 1968.

[2] J.M. Tenenbaum, *Accommodation in Computer Vision,* Ph.D. Thesis, Stanford University, 1970.

[3] R.A. Jarvis, *Focus optimization criteria for computer image processing,* Microscope, Vol. 24, No. 2, pp. 163-180, 1976.

[4] J.F. Schlag, A.C. Sanderson, C.P. Neumann, F.C. Wimberly, *Implementation of automatic focusing algorithms for a computer vision system with camera control,* Carnegie Mellon University, CMU-RI-TR-83-14, August, 1983.

[5] E. Krotkov, *Focusing,* International Journal of Computer Vision, Vol. 1, pp. 223-237, 1987.

[6] E. Krotkov, *Exploratory visual sensing with an agile camera,* Ph.D. Dissertation, TR-87-29, University of Pennsylvania, 1987.

[7] A. Pentland, *A New Sense for Depth of Field,* IEEE Transactions on Pattern Analysis and Machine Intelligence, Vol. 9, No. 4, pp. 523-531, July 1987.

[8] P. Grossmann, *Depth from Focus,* Pattern Recognition Letters, Vol. 5, pp. 63-69, 1987.

[9] T. Darrell and K. Wohn, *Pyramid Based Depth from Focus,* Proc. CVPR, pp. 504-509, 1988.

[10] M. Subbarao, *Efficient Depth Recovery through Inverse Optics,* Machine Vision for Inspection and Measurement, edited by H. Freeman, Academic Press, 1989.

[11] T. Ohta, K. Sugihara, and N. Sugie, *A Method for Image Composition using Image Variance,* Transactions of IECE, Vol. J66-D, No. 10, pp. 1245-1246.

[12] K. Kaneda, Y. Wakasu, E. Nakamae, E. Tazawa, *A Method of Pan-Focused and Stereoscopic Display Using a Series of Optical Microscopic Images,* Proc. of Fourth Symposium on Image Sensing Technologies in Industry, pp. 189-194, June, 1988.

[13] K. Torrance and E. Sparrow, *Theory for Off-Specular Reflection from Roughened Surfaces,* Journal of the Optical Society of America, No. 57, pp. 1105-1114, 1967.

[14] S. K. Nayar, K. Ikeuchi, T. Kanade, *Surface Reflection; Physical and Geometrical Perspectives,* Carnegie Mellon University, CMU-RI-TR-89-7, March, 1989.

[15] S. K. Nayar, *Shape from Focus,* Carnegie Mellon University, CMU-RI-TR-89-27, November, 1989.

[16] T. Ninomiya, M. Nomoto, Y. Nakagawa, *Automatic 2-1/2D Shape Inspection System for Via-Hole Fillings of Green Sheets by Shadow Image Analysis,* Proc. IEEE Intl. Conf. on Robotics and Automation, pp. 515-520, 1989.

[17] M. Born and E. Wolf, *Principles of Optics,* London:Pergamon, 1965.

[18] B. K. P. Horn, *Robot Vision,* MIT Press, 1986.

[19] G. Westheimer, *The Eye,* Medical Physiology, Thirteenth Edition, Mosby Co., 1974.